Investigation on the Structural Variation of Co−Cu Nanoparticles during the Annealing Process

Shin-Pon Ju*

Department of Mechanical and Electro-Mechanical Engineering, Center for Nanoscience and Nanotechnology, National Sun Yat-Sen University, Kaohsiung 804, Taiwan, Republic of China

Yu-Chieh Lo

Institute of Materials Science and Engineering, Center for Nanoscience and Nanotechnology, National Sun Yat-Sen University, Kaohsiung, Taiwan 804, Republic of China

Shih-Jye Sun

Department of Applied Physics, National University of Kaohsiung, Kaohsiung 800, Taiwan, Republic of China

Jee-Gong Chang

National Center for High-Performance Computing, No. 21, Nan-Ke 3rd Road, Hsin-Shi, Tainan, Taiwan, Republic of China

Received: May 27, 2005; In Final Form: September 9, 2005

This study uses molecular dynamics simulations to investigate the crystalline process of Co−Cu nanoparticles of high and low Co concentrations (5 and 25%) during the annealing process. The modified many-body tight-binding potential involving magnetic contribution is adopted to accurately model the Cu−Cu, Co−Co, and Co−Cu pair interactions. The Co−Co bond length increases, while the Co−Cu bond length decreases as the temperature gradually drops from 2000 K to the upper melting point. During that process, the Cu−Cu bond length remains constant and the value of the first peak of the radial distribution function (RDF) increases, which indicates that Cu atoms increase their short-range order by mutual rearrangement. At temperatures lower than the upper melting point, the bond length of each pair decreases while the value of the first peak increases as the temperature is continuously reduced. Because the kinetic energy of an individual atom is not enough for rearrangement, the variations of bond length and the first RDF peak can be attributed to the shrinking effect.

Introduction

The ferromagnetic properties of spintronics have considerable potential for a variety of industrial applications and have therefore attracted considerable attention in recent years. Spintronics is an emerging technology with many potential applications,[1] including giant magnetoresistance (GMR)[2] digital storage devices. The magnetic properties at the nanoscale are of particular interest. The high magnetoresistance properties of Co−Cu granular nanoparticles render them promising candidates for spintronics applications.[3,4] Diluted Co−Cu alloys with a larger nanoscale size exhibit ferromagnetic properties at room temperature.[5,6] From the experimental observation on the annealed Cu−Co samples of different Co concentrations, it has been proven that the atomic-level structure variations, such as the variation of the average bond length and the Co atom distribution inside the Co−Cu nanoparticle, have a significant influence on the magnetic properties of Co−Cu samples.[7] During the annealing process, since it is difficult to investigate the atomic-level structure variation of a Co−Cu nanoparticle directly using experimental approaches, numerical methods are commonly employed to obtain detailed insight into the atomic-level structure variation during the annealing process. Molecular dynamics (MD) simulation provides a powerful means of investigating atomic behaviors from an atomic viewpoint. Utilizing this technique, Shimono and Onodera found the critical cooling rate necessary to produce the amorphous state at different Al concentrations for the binary Ti−Al alloys.[8] By inspecting the vibration spectrum obtained from the Fourier cosine transform of the atomic velocity autocorrelation function, they also demonstrated that the excess of low frequency vibration modes in the amorphous state becomes weaker during the annealing process and disappears after crystallization. The effect of the cooling rate for the binary Ag−Cu alloy system on the atomic-level structure is also demonstrated by monitoring the variations of the chemical short-range-order (CSRO) parameter and local packing order from the common-neighbor analysis in MD simulations.[9] They concluded that an extremely high cooling rate is helpful to form an amorphous structure, while a homogeneous crystalline structure tends to form at lower cooling rates. Besides investigating the effect of the cooling rate, molecular dynamics simulation is also used to monitor the migration of the atoms with nearest-neighbor vacancies and conduct an analysis of the atomic jump mechanism in binary

* To whom correspondence should be addressed (Assistant Professor). E-mail: jushin-pon@mail.nsysu.edu.tw.

10.1021/jp052803k CCC: $30.25
Published on Web 10/15/2005

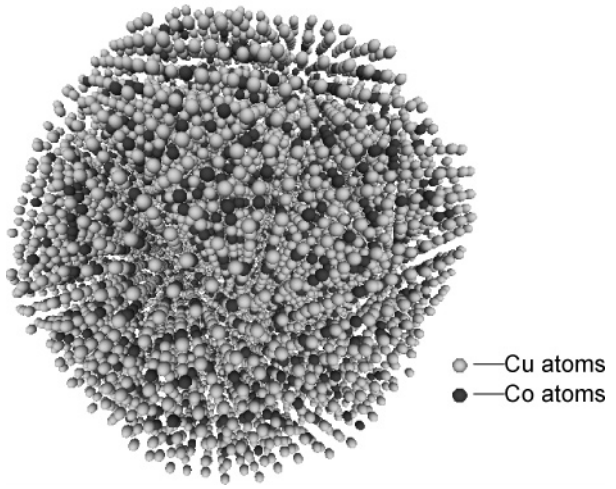

Figure 1. Schematic diagram of the Co−Cu nanoparticle in molecular dynamics simulation.

alloys.[10] In addition, the atomic dynamic behaviors and local structure variation of bimetallic nanoparticles at different temperatures and element concentrations can be accurately described by this method using a suitable potential function.[11,12]

From the discussions above, it is clear that MD simulation serves as an essential technique for the investigation of the fundamental molecular behaviors at an atomic level. In our previous study, we successfully used molecular dynamics simulation to obtain the distributions of Co atoms within granular Co−Cu nanoparticle alloys and then applied those Co distributions to explore the temperature dependency of the magnetization properties of diluted Co−Cu alloys by the molecular Wiese mean field theory.[13] The simulation results compare favorably with the experimental results presented qualitatively in the literature.[14] Since both the experimental and simulation results display strong evidence that the atomic-level structure in a Co−Cu nanoparticle has a direct influence on its magnetic properties, it is useful to investigate the atomic-level variation of Co and Cu arrangements at different temperatures by MD simulation in order to compensate for the limitations of the experimental approaches. In the present study, the modified tight-binding potential, which involves the magnetic contribution, is used to accurately model the Cu−Cu, Co−Cu, and Co−Co pair interactions in Co−Cu nanoparticles of 5 and 25% Co concentrations. At different temperatures, the rearrangements of Co and Cu atoms as well as the bond length variations are investigated in detail.

Simulation Model

Figure 1 presents a schematic diagram of a Co−Cu nanoparticle. The present simulations consider two individual Co−Cu nanoparticles including 9597 atoms, whose Co concentrations are 5 and 25%. The initial structures are arranged in a face-centered cubic (fcc) configuration with a random distribution of Co atoms embedded in a Cu matrix. An annealing temperature of 2000 K for 400 ps and a following cooling rate of 1 K/ps are used to model the annealing process of Co−Cu nanoparticles. The present simulations employ the velocity Verlet algorithm[15] to calculate the trajectories of the atoms, and the scaling method is adopted during the simulation to control the system temperature.

The simulations consider a range of atomic interactions, namely, interactions between the Cu atoms, interactions between the Co atoms, and interactions between the Cu and Co atoms. All atomic interactions are modeled by the many-body tight-binding potential modified by Levanov et al.[16] as follows:

$$E_i = -\left\{\sum_j \xi^2 \exp\left[-2q\left(\frac{r_{ij}}{r_0} - 1\right)\right]\right\}^{1/2} + \sum_j \left[A^1 \exp\left(\frac{r_{ij}}{r_0} - 1\right) + A^0\right] \exp\left[-p\left(\frac{r_{ij}}{r_0} - 1\right)\right] \quad (1)$$

The first term, an attractive part, commences by summing the band energy which is characterized by the second moment of the d-band density of state. The second term, a pairwise repulsive part, shows a modified form of the Born−Mayer type in the original tight-binding potential.[17] Furthermore, the interaction force on atom i is expressed by the following formula:

$$\bar{F}_i = \sum_{j \neq i} \left(\frac{\partial E_i}{\partial r_{ij}} + \frac{\partial E_j}{\partial r_{ij}}\right) \frac{\bar{r}_{ij}}{r_{ij}} \quad (2)$$

The parameters for the Cu element are determined from the experimental values, including the cohesive energy, lattice parameter, bulk modulus, and two shear elastic constants, C_{44} and $C' = 2(C_{11} - C_{12})$, respectively. The parameters of Co−Co and Co−Cu are fitted from the results of first-principle Korringa−Kohn−Rostoker (KKR) calculation. This modified tight-binding potential can more accurately model the interface properties of the Co−Cu binary system and describe the Co−Cu bonds than the original tight-binding potential. Moreover, the modified version can derive more accurate forces which involve magnetic contribution. The modified tight-binding potential is considered as one type of short-range potential because this many-body potential only considers the interaction between a reference atom and its first neighbor atoms. From the observation of the radial distribution profiles discussed in the Results and Discussion section of this study, a prominent first peak exists at each temperature modeled—above, below, and at the melting point—because short-range orders exist even at a high temperature. Moreover, Levanov et al. also found this potential can accurately model the interface and surface behavior of a Co−Cu alloy which reflects the burrowing of Co nanoparticles in Cu substrate, corroborating an experimental observation.[18] As described above, although the Co−Cu nanoparticles do not have good long-range lattice ordering and a large surface area, this potential is appropriate to model the atomic interaction in Co−Cu nanoparticles. The parameters of the modified tight-binding potential related to Cu and Co, which are used in the current simulation, are listed in Table 1.

TABLE 1: Parameters Used in the Modified Tight-Binding Potential

parameter	A^1 (eV)	A^0 (eV)	ξ (eV)	p	q	r_0 (Å)
Cu	0.0	0.086	1.224	10.960	2.278	2.556
Co	−0.852	0.139	1.5247	7.679	2.139	2.378
Co−Cu	−1.905	−0.049	0.7356	8.183	3.344	2.405

Result and Discussion

Figure 2 shows the variation of the cohesive energy and the corresponding temperature during the annealing process. As can be seen from Figure 2, the cohesive energy of Co−Cu nanoparticles of higher Co concentration is larger than that of lower Co concentration at all temperatures. The cohesive energy of the Co element is 4.386 eV larger than that of the Cu element, 3.544 eV, so the cohesive energies of a Co−Cu nanoparticle

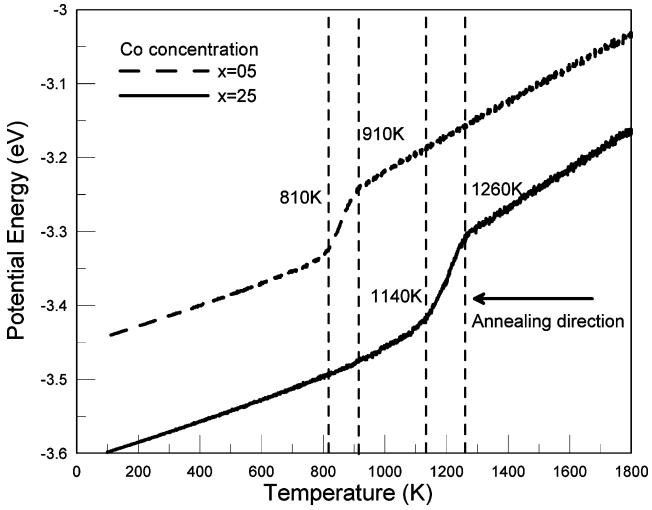

Figure 2. Variations of average potential energy at different temperatures for 5 and 25% Co concentrations. The dashed lines indicate the upper and lower melting points.

increase with its Co concentration. An abrupt energy drop occurs at 910 and 1260 K for 5 and 25% Co concentration Co−Cu nanoparticles, respectively, representing the respective melting points. This could be attributed to the transition of Co−Cu nanoparticle from an amorphous structure to a crystalline arrangement as the temperature drops below the melting point. At 810 and 1140 K for 5 and 25% Co concentration curves, the crystalline processes end and the shrinking of the Co−Cu nanoparticles leads to a gradual increase of cohesive energy as the temperature continues to decrease. The melting points for Co−Cu bulk alloys at 5 and 25% Co concentrations are about 1373 and 1623 K.[19] Comparing our simulation results to bulk material, it is obvious that the melting point of bulk material at the same Co concentration is significantly higher than a Co−Cu alloy with a higher surface−volume ratio such as a nanoparticle in this study. This phenomenon is also found in related studies for Au nanoparticles.[20] The melting point is lower for a smaller Au nanoparticle because the bonding energy is smaller for a smaller Au nanoparticle having a higher surface−volume ratio.[20,21] For convenience in describing our simulation results, the upper melting point and the lower melting point are used to represent the temperature at which the crystalline process starts and ends. Clearly, both the upper and lower melting points of higher Co concentration are larger than those of lower Co concentration. Radial distribution functions (RDFs) are used to investigate the structural transition between the upper and lower melting points. The RDF is usually adopted to investigate the microstructure of bulk materials which adopt the periodic boundaries in each dimension or layer structures which employ the periodic boundaries in the plane directions. In these cases, the periodic boundaries allow the observation of both long- and short-range pair correlations of the system by investigating the variation of the RDF. In this study, what we focus on is observing the short-range correlation between Co−Co, Cu−Cu, and Cu−Co pairs, rather than their long-range correlations. Consequently, it is more convenient to use the first few peaks of RDF profiles to investigate the short-range variations of Co−Co, Cu−Cu, and Cu−Co pairs. Parts a and b of Figure 3 depict the radial distribution function at the upper melting point, the lower melting point, and an intermediate temperature between these two temperatures for Co−Cu nanoparticles of 5 and 25% Co concentrations, respectively. At the upper melting point and the intermediate temperature, the RDF profiles for 5 and 25% Co concentrations are very similar, where

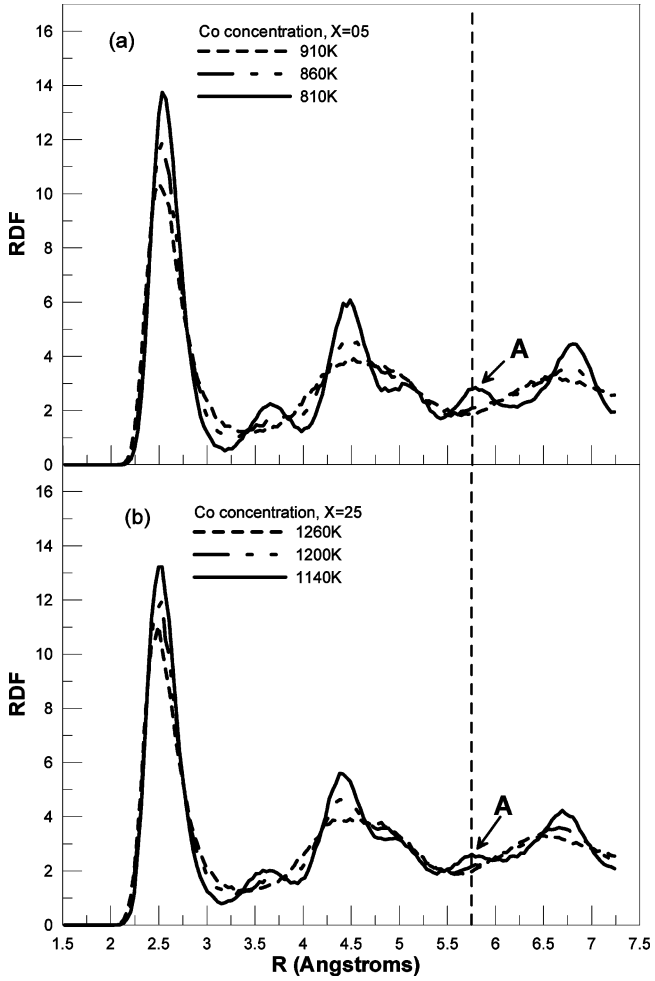

Figure 3. Radial distribution function profiles at the upper melting point, the lower melting point, and an intermediate temperature for (a) 5% and (b) 25% Co concentrations.

only a short-range order of atomic arrangement exists rather than a long-range order. There is no corresponding specific lattice structure at both the upper melting point and the intermediate temperature. At the lower melting point, the RDF profiles show the long-range order of atomic arrangement. For the lower Co concentration, the relative positions of the peaks on the horizontal axis of the RDF profile reveal that the majority of the Co−Cu nanoparticle is in the fcc arrangement, because 95% of the atoms are Cu atoms having their most stable structure in the fcc arrangement. Although the RDF profile for a 25% Co concentration is similar to the 5% Co profile, some small discrepancies in the RDF profiles for low and high Co concentrations show a larger fraction of the hexagonal close-packed (hcp) structure exists in Co−Cu nanoparticles of higher Co concentration than the fraction of lower Co concentration. For example, the peak labeled A in Figure 3a is more prominent than that in Figure 3b and the RDF profiles for perfect hcp and fcc lattice structure show the peak value at label A is relatively smaller for the hcp structure compared with that of the fcc structure.

Parts a and b of Figure 4 depict the variations of Cu−Cu, Co−Co, and Co−Cu bond lengths at different temperatures for 5 and 25% Co concentrations, respectively. Because there is only a small number of Co atoms in Co−Cu nanoparticle of 5% Co concentration in Figure 4a, the fluctuation of Co−Co bond length at different temperatures is more apparent. The Co−Co, Cu−Co, and Cu−Cu bong length profiles for both 5

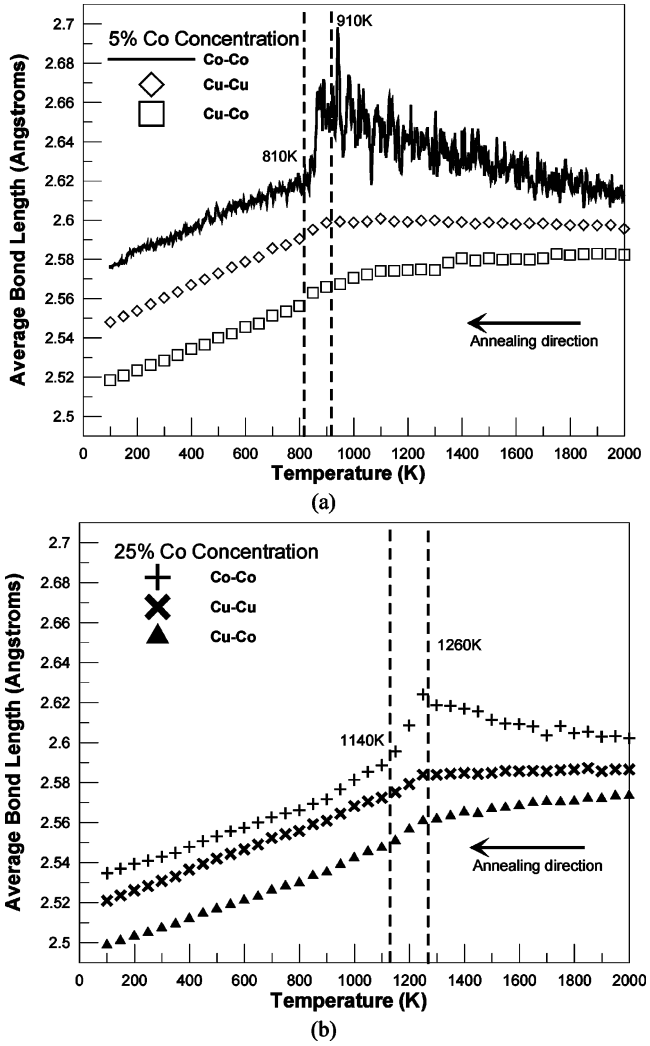

Figure 4. Cu−Cu, Co−Co, and Co−Cu bond length variations at different temperatures for (a) 5% and (b) 25% Co concentrations. The dashed lines indicate the upper and lower melting points.

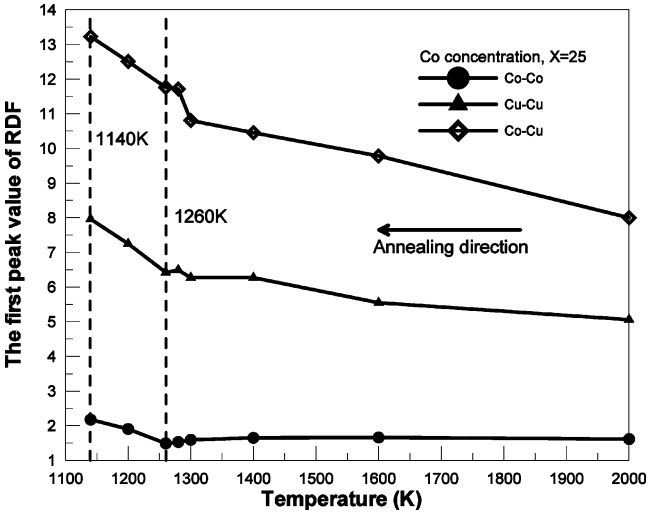

Figure 5. Variations of the RDF first peaks of Co−Co, Cu−Cu, and Co−Cu pairs at different temperatures. The dashed lines indicate the upper and lower melting points.

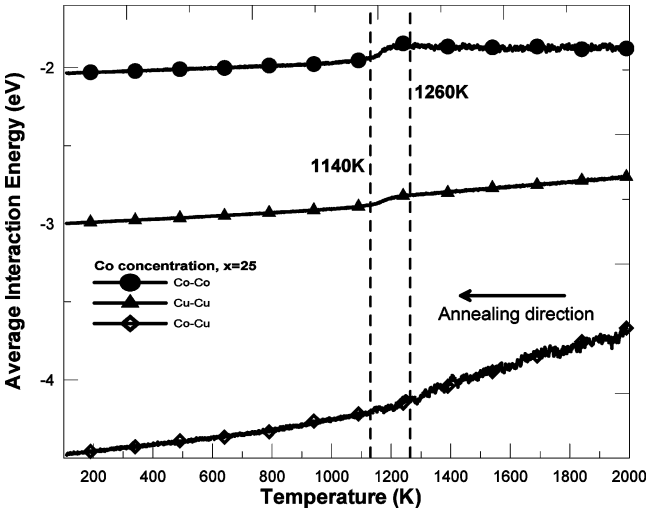

Figure 6. Variations of the average interaction energies between the reference Cu atom with its neighbor Cu atoms and the reference Co atom with its neighbor Co and Cu atoms. The dashed lines indicate the upper and lower melting points.

and 25% Co concentrations are similar, as shown in Figure 4a and b. At temperatures over the upper melting point, the Cu−Cu bond length remains a constant value. As the temperature decreases toward the upper melting point, the Co−Co bond length increases, while the Co−Cu length decreases. After the temperatures of Co−Cu nanoparticles drop lower than the upper melting temperature, the lengths of these three bond lengths decrease with the temperatures. In Figures 5 and 6, the value of the first RDF peak and the average interaction energy of the reference atom in the RDF calculation with its neighbor atoms are adopted to explain the mechanism of bond variation with the temperature shown in Figure 4a and b. Because the tendencies of bond length variations are similar for temperatures in 5 and 25% Co concentrations, only the Co−Cu nanoparticle of 25% Co concentration is considered in Figures 5 and 6. The vertical axis of Figure 5 represents the value of the first peak of the RDF shown in Figure 3b. The value of the first peak indicates the average number of the first neighbor atoms around the reference atom, while in Figure 6 the vertical axis expresses the average interaction energy of the reference atom with its neighbor atoms. As seen in Figure 5, higher Cu concentration in a Co−Cu nanoparticle leads to the largest first peak value for the Co−Cu pair, the smallest first peak value for the Co−Co pair, and the intermediate value for the Cu−Cu pair at all temperatures. In Figure 6, the value of the first RDF peak in Figure 5 also reveals the strength of the interaction between the reference atom and its neighbor atoms, because the reference atom has a stronger interaction with the neighbor atoms whose type causes the larger first peak value of the reference atom. Consequently, on average, a Co atom interacts much more strongly with neighbor Cu atoms than neighbor Co atoms in the Co−Cu nanoparticle. At the range of temperatures from 2000 K down to a melting point of 1260 K, Cu atoms rearrange to form a more ordered structure inside the Co−Cu nanoparticle as the temperature continuously decreases, leading to the increase of the RDF first Cu−Cu peak value and Cu−Cu interaction energy. It should be noted that the Cu−Cu bond length remains almost constant, which reveals that it is the rearrangement of Cu atoms rather than the shrinking of the nanoparticle that causes the increase of the RDF peak and interaction energy of the Cu−Cu pair as the temperature decreases. Because the interaction energy of Co−Cu is higher than the Co−Co interaction energy, some Cu atoms having first neighbor Co atoms also tend to rearrange with other Cu atoms and these arrangements force the Co−Co bond length of some small Co clusters to increase inside the Co−Cu nanoparticle.

As a consequence, the Co−Co bond length increases as the temperature decreases, resulting in the decreasing tendency of the Co−Co energy and the Co−Co RDF first peak. Figures 5 and 6 demonstrate that the Co−Co interaction will be significantly influenced by the variation of the rearrangement of Cu atoms because the Co−Co interaction energy is smaller than Co−Cu interaction energy. At temperatures lower than the upper melting point, the amorphous structure gradually transforms into a crystalline structure as the temperature decreases. As the temperature decreases, the shrinking effect of the Co−Cu nanoparticle causes the bond length of each pair to decrease, which results in an increase of the RDF peak value and interaction energy of each pair.

Conclusion

This paper investigates the annealing process of Co−Cu nanoparticles with both high and low Co concentrations using a molecular dynamics simulation from an atomic viewpoint. The cohesive energy and the melting point are significantly tied to the concentration of Co atoms. A Co−Cu nanoparticle of higher Co concentration has a higher cohesive energy and a correspondingly higher melting point. From close inspection of the RDF profiles, a larger fraction of hcp structure appears in Co−Cu nanoparticles for the higher Co concentration. This study also investigates the variations of each kind of bond at different temperatures, including Cu−Cu, Co−Cu, and Co−Co pairs. Because the Co−Co interaction energy is smaller than the Co−Cu interaction energy, the Co−Co interaction will be significantly influenced by the variation of the rearrangement of Cu atoms. At temperatures over the upper melting point, the Co−Co bond length increases, whereas the Co−Cu bond length has a tendency to decrease as the temperature continuously decreases. However, the Cu−Cu bond length remains constant and Cu atoms rearrange to increase the short-range order. This in turn leads to an increase of the RDF first peak value for the Cu−Cu and Co−Cu pairs but causes a decrease in the RDF first peak value for the Co−Co pair. As the temperature gradually decreases from the upper melting point, the amorphous structure gradually transforms into a crystalline structure. Because the kinetic energy of an individual atom is not sufficient for rearrangement at this time, the shrinking effect of the Co−Cu nanoparticle causes the bond length of each pair to decrease, which results in an increase of the RDF peak value and interaction energy of each pair.

Acknowledgment. The authors gratefully acknowledge the support provided to this research study by the Center for Nanoscience and Nanotechnology of National Sun Yat-Sen University and the National Science Council of the Republic of China under Grant No. NSC 93-2212-E-110-022.

References and Notes

(1) Žutić, I.; Fabian, J.; Das Sarma, S. *Rev. Mod. Phys.* **2004**, *76*, 323.
(2) Baibich, M. N.; Broto, J. M.; Fert, A.; Nguyen Van Dau, F.; Petroff, F.; Etienne, P.; Creuzet, G.; Friederich, A.; Chazeles, J. *Phys. Rev. Lett.* **1988**, *61*, 2472.
(3) Berkowitz, A. E.; Mitchell, J. R.; Carey, M. J.; Young, A. P.; Zhang, S.; Spada, F. E.; Parker, F. T.; Hutten, A.; Thomas, G. *Phys. Rev. Lett.* **1992**, *68*, 3745.
(4) Xiao, J. Q.; Jiang, J. S.; Chien, C. L. *Phys. Rev. Lett.* **1992**, *68*, 3749.
(5) Fan, X.; Mashimo, T.; Huang, X.; Kagayama, T.; Chiba, A.; Koyama, K.; Motokawa, M. *Phys. Rev. B* **2004**, *69*, 094432.
(6) Hickey, B. J.; Howson, M. A.; Musa, S. O.; Tomka, G. J.; Rainford, B. D.; Wiser, N. *J. Magn. Magn. Mater.* **1995**, *147*, 253.
(7) Cezar, J. C.; Tolentino, H. C. N.; Knobel, M. *Phys. Rev. B* **2003**, *68*, 054404.
(8) Shimono, M.; Onodera, H. *Mater. Sci. Eng.* **2001**, *304*−*306*, 515−519.
(9) Sheng, H. W.; He, J. H.; Ma, E. *Phys. Rev. B* **2002**, *65*, 184203.
(10) Oramus, P.; Massobrio, C.; Kozubski, R.; Pierron-Bohnes, V.; Cadeville, M. C.; Pfeiler, W. *Comput. Mater. Sci.* **2003**, *27*, 186−190.
(11) Huang, S. P.; Mainardi, D. S.; Balbuena, P. *Surf. Sci.* **2003**, *545*, 163−179.
(12) Rodriguez, J. L.; Montejano-Carrizales, J. M.; Yacaman, M. J. *Appl. Surf. Sci.* **2003**, *219*, 56−63.
(13) Sun, S. J.; Ju, S. P.; Lo, Y. C.; Lin, J. S. *J. Appl. Phys.* **2005**, *97*, 094308.
(14) Childress, J. R.; Chien, C. L. *Phys. Rev. B* **1991**, *43*, 8089.
(15) Allen, M. P.; Tildesley, D. J. *Computer Simulation of Liquid*; Clarendon Press: Oxford, U.K., 1991; Chapter 3.
(16) Levanov, N. A.; Stepanyuk, V. S.; Hergert, W.; Bazhanov, D. I.; Dederichs, P. H.; Katsnelson, A.; Massobrio, C. *Phys. Rev. B* **2000**, *61*, 2230.
(17) Cleri, F.; Rosato, V. *Phys. Rev. B* **1993**, *48*, 22.
(18) Zimmermann, C. G.; Yeadon, M.; Nordlund, K.; Gibson, J. M.; Averback, R. S.; Herr, U.; Samwer, K. *Phys. Rev. Lett.* **1999**, *83*, 1163.
(19) Gente, C.; Oehring, M.; Bormann, R. *Phys. Rev. B* **1993**, *48*, 13244.
(20) Shim, J. H.; Lee, B. J.; Cho, Y. W. *Surf. Sci.* **2002**, *512*, 262−268.
(21) Rogan, J.; Ramirez, R.; Romero, A. H.; Kiwi, M. *Eur. Phys. J. D* **2004**, *28*, 219−228.